A light-mediated, 3D-printable, and self-healable polymer electrolyte for lithium batteries

ADVANCED FUNCTIONAL MATERIALS

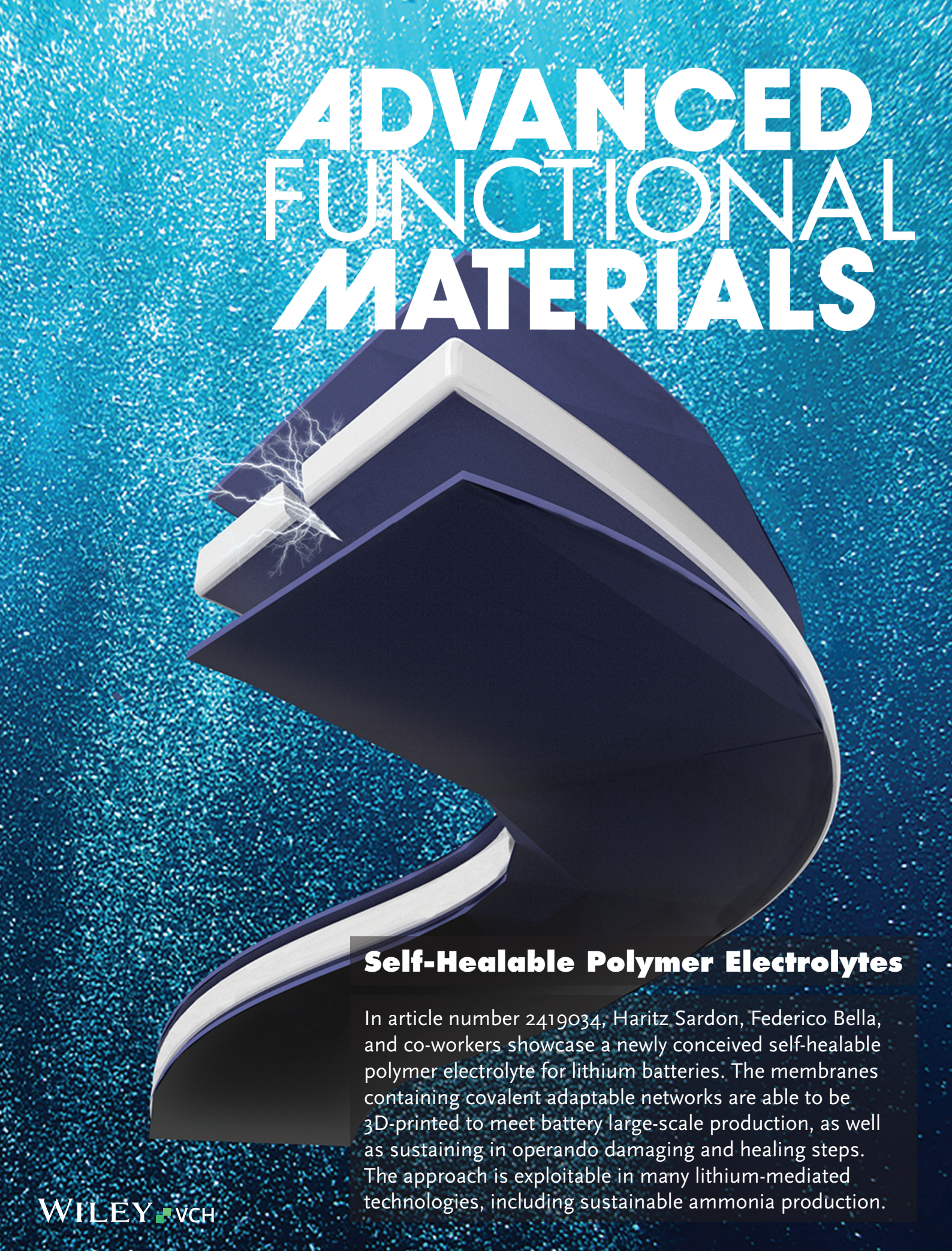

Self-Healable Polymer Electrolytes

In article number 2419034, Haritz Sardon, Federico Bella, and co-workers showcase a newly conceived self-healable polymer electrolyte for lithium batteries. The membranes containing covalent adaptable networks are able to be 3D-printed to meet battery large-scale production, as well as sustaining in operando damaging and healing steps. The approach is exploitable in many lithium-mediated technologies, including sustainable ammonia production.

WILEY VCH

ADVANCED FUNCTIONAL MATERIALS
www.afm-journal.de

A Light-Mediated, 3D-Printable, and Self-Healable Polymer Electrolyte for Lithium Batteries

Fermin Elizalde, Sabrina Trano, Jon Ayestarán, Xabier Lopez de Pariza, Robert Aguirresarobe, Carlotta Francia, David Mecerreyes, Haritz Sardon, and Federico Bella**

Self-healing materials solutions and rapid prototyping approaches are actively searched to improve the safety and the production processes of batteries at the gigascale. Here, a self-reparable polymer electrolyte designed into 3D-printable ink formulation for digital light processing is shown. For this purpose, covalent adaptable networks containing hindered urea dynamic bonds end-capped with photopolymerizable methacrylate groups are designed and investigated in terms of dynamicity and self-healing properties. Electrochemical performance of the electrolytes is tested and compared with a commercially available benchmark, showing in all cases superior electrolyte uptake, ionic conductivities, and full specific capacity recovery after being cut in operando. This work brings the first self-healable and 3D-photoprinted electrolyte system for lithium batteries, at once ensuring safety, performance, and upscalability; the concept is also exploitable in lithium-mediated ammonia electrosynthesis.

1. Introduction

Energy harvesting and storage have been playing an important role in the global low/zero-carbon energy strategy.[1–3] Researchers are exploring new materials to ensure highly performant and effective electrochemical energy storage and conversion devices, such as batteries, fuel cells, or supercapacitors.[4,5] Lithium-ion batteries (LIBs) have been employed in several kinds of portable electronic devices, electric vehicles, and implantable medical devices.[6–8] Using lithium metal as an anode material is a promising approach to increase the energy storage capacity of the battery technology,[9–11] as well as for other technologies, e.g. lithium-mediated nitrogen reduction to safely produce ammonia and fertilizers.[12] However, the main drawback of lithium-metal batteries (LMBs) is represented by the safety issues associated with the undesired lithium dendrite growth during electrochemical plating and stripping.[13] Throughout lithium deposition/stripping, volume changes are given in the metal anode, leading to cracks and defects that concentrate Li^+ flux and promote lithium dendrites growth,[14] leading to battery failure. Consequently, the cycling life of these devices is limited.[15] To face this issue, self-healing electrodes and electrolytes are being developed as a potential solution, as they can boost the cycling life of electrochemical devices and increase their safety since dendrite growth could be diminished.[13,16,17]

From the chemical point of view, supramolecular interactions have been mainly employed to develop self-healing polymers for batteries. Particularly, hydrogen bonds and ionic interactions have gained most of the attention, being applied as binders and, in some literature papers, as polymer electrolytes.[18–20] Recently, covalent adaptable networks (CANs) have emerged as a new alternative for introducing autonomous repairing properties. These dynamic networks are particularly interesting as they offer greater mechanical stability, before and after being repaired, than the counterparts crosslinked via supramolecular interactions. Moreover, the design of these dynamic networks could provide enlarged stability at usage conditions while fast-healing ability under given stimuli. For this purpose, the proper choice of dynamic covalent bonds and network structure is crucial.[21]

Initially, boronic esters[22] and disulfide bonds[23] were studied as chemical motifs to provide dynamicity in polymer electrolytes. However, they are usually expensive, their implementation requires the preparation of a specifically designed monomer, and their versatility is limited as they provide little tunability in the dynamic character of the chemical bond. More recently, we have investigated the use of hindered urea bonds (HUBs)[18] to prepare

F. Elizalde, J. Ayestarán, X. L. de Pariza, R. Aguirresarobe, D. Mecerreyes, H. Sardon
POLYMAT
University of the Basque Country UPV/EHU
Joxe Mari Korta Center Avda. Tolosa 72,
Donostia-San Sebastian 20018, Spain
E-mail: haritz.sardon@ehu.es
S. Trano, C. Francia, F. Bella
Department of Applied Science and Technology
Politecnico di Torino
Corso Duca degli Abruzzi 24, Turin 10129, Italy
E-mail: federico.bella@polito.it
The ORCID identification number(s) for the author(s) of this article can be found under https://doi.org/10.1002/adfm.202419034

DOI: 10.1002/adfm.202419034

self-healable polymer electrolytes. This dynamic bond facilitates an easy implementation into the polymer network in a cost-effective manner. In addition, HUBs dynamicity can be modified by appropriately selecting the substituent of the secondary amine, as reported by Chen et al.[24] and other groups.[12] One of the most important limitations of the strategy that we developed was that the formation of the polymer electrolyte membranes was based on a thermal process, not only limiting the attainable dimensional reproducibility and complexity, but also increasing production times. In this regard, advanced manufacturing technologies, such as additive manufacturing (AM), are crucial when well-defined and reproducible morphologies are required.

AM, commonly named 3D printing, has brought significant advancements and transformative changes in manufacturing processes. AM offers a range of advantages including design freedom for complex geometries, rapid prototyping, cost-effectiveness, and – more importantly – the potential for straightforward customization and personalization.[25] Highly detailed and accurate printings can be achieved with a wide range of materials for different applications.[26] AM methods have become particularly interesting to develop systems applicable in the future of energy storage devices.[27] In particular, 3D printing for LIBs and LMBs has been recently demonstrated for the preparation of cathodes,[28] anodes,[29] inorganic solid electrolytes,[30] and flexible architectures;[31] also, a comprehensive review on this topic has been just published by Sida et al.,[32] where two main outstanding achievements emerge: i) a flexible control of the electrode structure on a microscopic scale, which is crucial to improve the energy density of miniaturized devices; ii) solid electrolyte consisting of periodically arranged vertical channels and hierarchically porous filaments that facilitate the liquid electrolyte infiltration and rapid ion diffusion for high-performance cells.

So far, direct ink writing (DIW) has been the most applied method in that field due to the wide range of employed materials, the simplicity of the process, and the low cost. Nevertheless, high active mass loadings into the slurry promote the increase of the viscosity in the ink, becoming a technical issue. Furthermore, structures produced through DIW are often restricted in terms of height due to the inherent limitations of stacking multiple layers, especially when the inks do not solidify fast and completely.[33] An underutilized alternative to DIW is vat photopolymerization (VP).[34] VP presents a cost-effective, readily processable, and high-resolution method to print any type of polymeric material. One of the greatest advances of VP, besides the high resolution, is the reduced material waste that is generated using this technology. The significant advantage of VP is that fabricated electrodes can have smaller feature sizes and more complex geometries than those made via other AM methods enlarging the attainable properties. Moreover, reduced waste is an important aspect considering the increasing demand for energy storage devices.[35] While the benefit of VP to fabricate self-healable polymer electrolytes is out of the discussion, the biggest challenge faced by VP is the lack of inks with desired functionality that meet the requirements to be printable, such as low viscosity to minimize suction pressure and adhesion,[36] or fast curing times to achieve high resolution in a cost-efficient fashion.[37] Therefore, relatively few examples of printed polymer electrolytes by VP have been reported so far,[38,39] and as far as we are aware they do not have self-healing capabilities. Within this context, among VP processes digital light processing (DLP) is a well-established method, due to excellent feature resolution and building speed.[40]

In this article, a new generation of high ion-conductive DLP printable polymer electrolytes based on hindered urea dynamic chemistry was investigated (**Scheme 1**). The use of UV-light to trigger the photopolymerization enables the rapid production of polymer electrolytes, making it compatible with additive manufacturing methods, such as DLP. In the first stage, we end-capped a low viscosity and high conductivity hindered urea-urethane oligomer with photocurable methacrylic moieties. Subsequently, we investigated its UV-photopolymerization in the form of membranes or 3D-printed objects. Then, the ionic conductivity, electrochemical stability, and self-healing properties of the obtained poly(urea-urethane) polymer electrolyte were investigated. Finally, its performance in lab-scale LMBs was assessed, including the use of VP in the fabrication process of the cell.

2. Results and Discussion

2.1. Synthesis of Dynamic UV-Curable HUB-PU Poly(Urea-Urethane) Networks

Novel poly(urea-urethane) networks were obtained through the synthetic route shown in **Figure 1A**. First, dynamic HUB-containing trimers are synthesized, reacting two equivalents of aliphatic isocyanate (hexamethylene diisocyanate, HDI) with one equivalent of *N,N′*-di-tert-butylethylenediamine. This amine has been selected as –in previous work –it showed the best dynamic behavior according to the bulkiness of the isopropyl substituents.[41] The dynamic trimers were then reacted with poly(ethylene glycol) (PEG) diols using an organotin catalyst (i.e., dibutyltin dilaurate – DBTDL). This polyol has been used as it can provide the highest conductivity values with reduced viscosity. In the last step, 2-hydroxyethyl methacrylate (HEMA) was added to end-cup oligomer chains, yielding a difunctional oligomer reactive toward UV-induced radical photopolymerization, using 2,2-dimethoxy-2-phenylacetophenone (DMPA) as a photoinitiator. These were characterized by ^{1}H nuclear magnetic resonance (NMR) to confirm their chemical structure; spectra are shown in Figures S1 and S2 (Supporting Information). Besides, the curing behavior of every step has been followed by Fourier-transform infrared (FTIR) spectroscopy, as shown in Figure 1B. As it can be seen in the spectra, in the first step the isocyanate stretching band at 2256 cm^{-1} completely disappeared (grey band) and a new band corresponding to the formation of the urea group appeared at 1618 cm^{-1} (blue band), followed by the corresponding band of urethane group at 1717 cm^{-1} (orange band). Subsequent to the photopolymerization step, the HEMA-derived methacrylate band was expected to be consumed, although it was not observed due to overlapping with the urea group present in the compound. To confirm the methacrylate conversion and, therefore, the curing process, photo-differential scanning calorimetry (DSC) experiments were carried out. These new data revealed that, under UV-light irradiation (370 nm), high monomer conversion (>85%) was achieved for all the tested formulations within the first minute of irradiation (Figure S3, Supporting Information). Besides, the formation of the dynamic thermoset material was confirmed by gel content experiments, where values

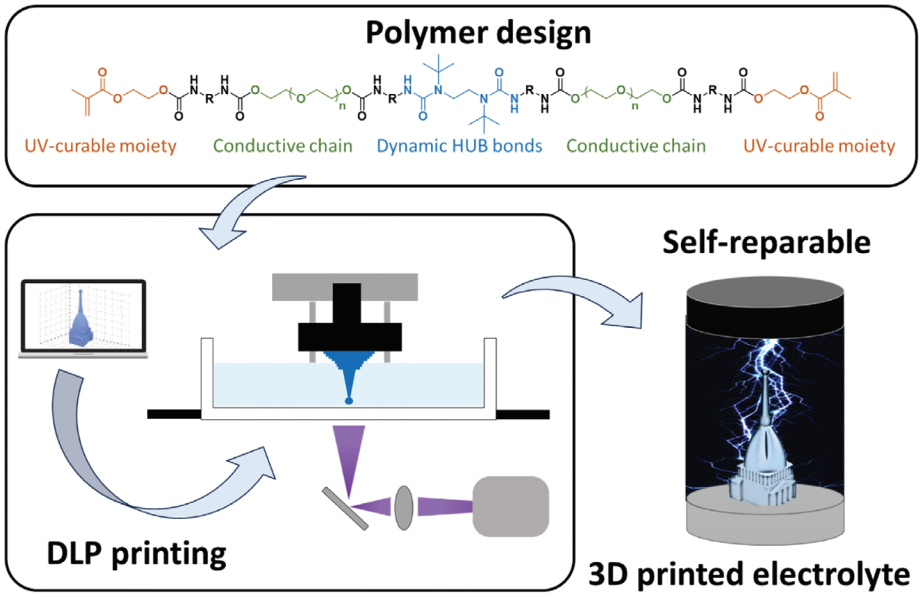

Scheme 1. Synthesized polymer structure and newly conceived strategy in this work.

≈40% were obtained, due to the dynamic behavior of the bulky moiety.

To investigate the impact of varying the amounts of dynamic bonds on electrochemical performance, the *N,N'*-di-tert-butylethylenediamine/PEG2100 ratio was adjusted to create three distinct formulations, as outlined in Table S1 (Supporting Information) (entries 1–3). Furthermore, to compare formulations containing PEG segments of different molecular weights (i.e., M_n = 2100 and 4300 g mol^{-1}), an additional composition (i.e., entry 4) was synthesized while maintaining the maximum quantity of dynamic bond (i.e., 1.5 eq. of *N,N'*-di-tert-butylethylenediamine). From now on, these polymeric networks will be abbreviated as polyPU-HUB.

2.2. Self-Healing Properties and Dynamicity of Polypu-HUB Networks

HUBs have been employed in this work due to their low dissociative temperature needed for the exchange. **Figure** 2A shows

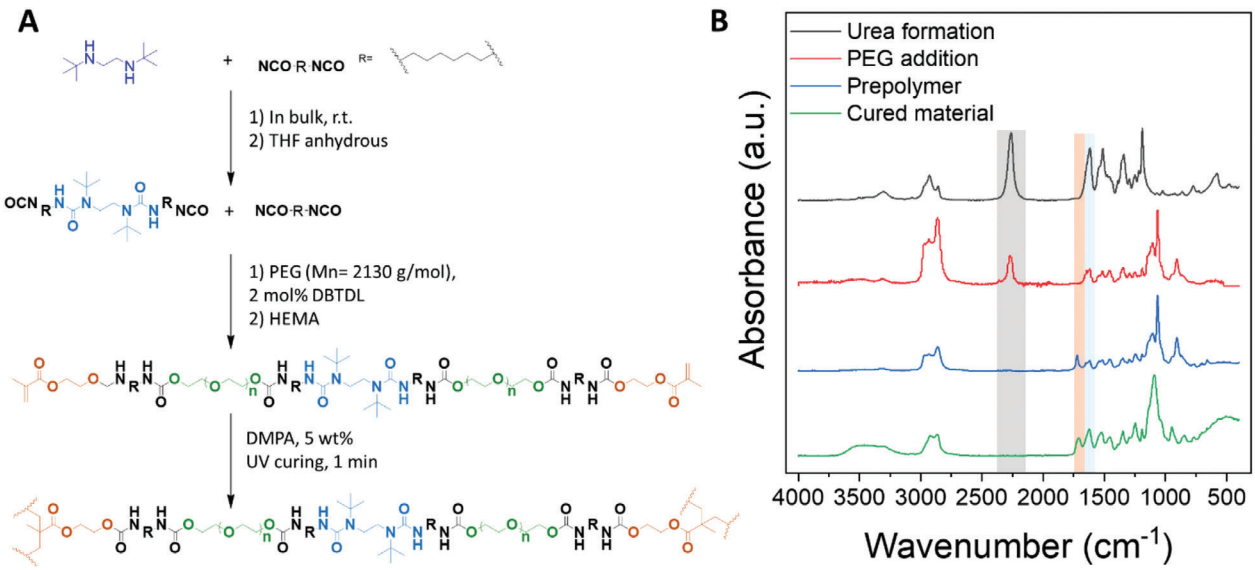

Figure 1. A) Synthetic procedure for obtaining cross-linked aliphatic polyurethanes with dynamic crosslinking points based on HUBs. B) Representative FTIR spectra of the reaction between *N,N'*-di-tert-butylethylenediamine and HDI (black spectrum). The addition of PEG (M_n = 2100 g mol^{-1}) to the mixture (red spectrum) and the spectrum obtained for the prepolymer formation (blue spectrum) are also shown. Finally, the green spectrum corresponds to the final poly(urea-urethane) film crosslinked by UV light for 45 s.

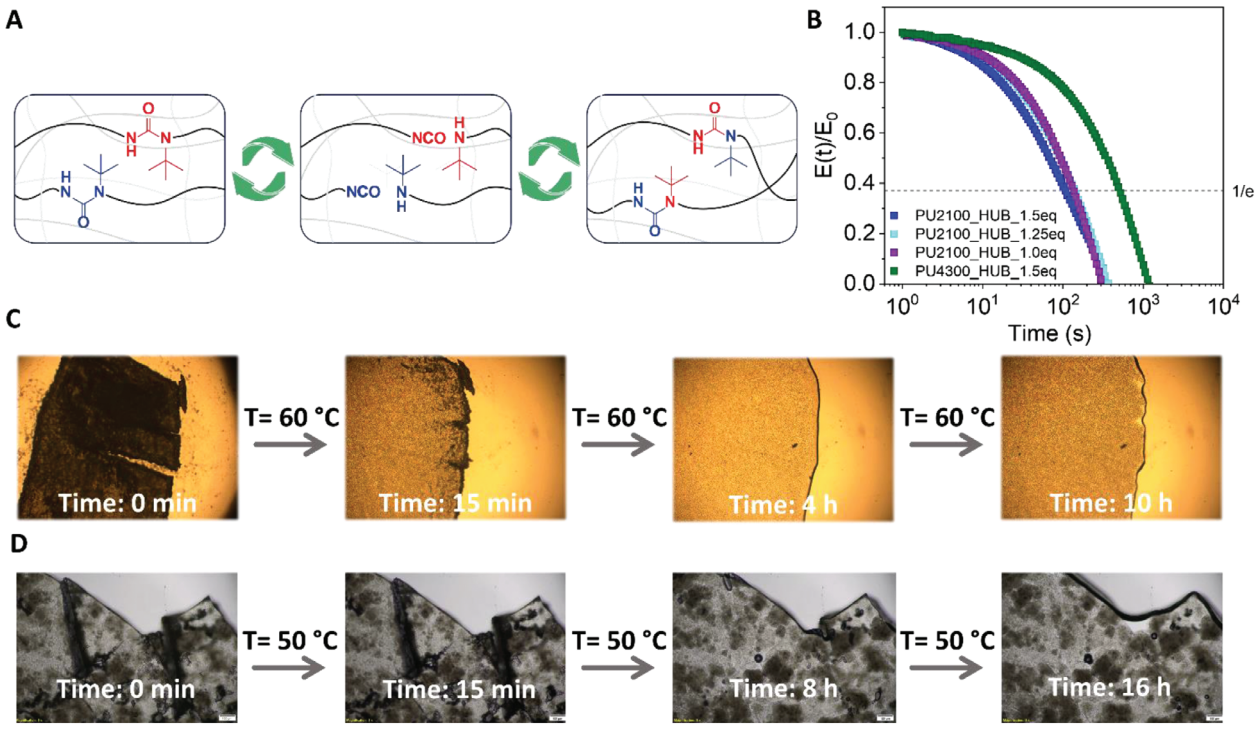

Figure 2. A) HUB dissociative exchange equilibrium. B) Stress-relaxation analysis for all the formulated membranes, performed at 120 °C. C) Scratch disappearance in PU2100_HUB_1.5eq network membrane after being kept 10 h at 60 °C C) Rate performance of a cell assembled with the PEG2100_HUB_1.5eq. composition and D) 16 h at 50 °C with little pressure (applied by closing two glass pieces with paper clips).

the dissociative mechanism inherent to this dynamic bond. Due to the bulkiness of the amine substituent, the formed urea can dissociate in the original free isocyanate and substituted amine as reported by Cheng and coworkers.[21] Once this step is given, these free functional groups can react with other isocyanates and amines, triggering a network rearrangement process, which leads to self-healing behavior.

It is well established that exchangeable bonds allow chain rearrangement in CANs, providing the expected self-healable properties to the material. For this reason, the rheological properties of the three different polymer networks were investigated. Under continuous strain (5%), the decrease of the moduli is given when internal chain reorganization takes place. Based on the obtained stress-relaxation times (τ) (Figure 2B), it can be concluded that all the compositions that had initial storage modulus in the range of 0.4–12 MPa (Figure S4, Supporting Information) stress-relaxed very fast at 120 °C. The main difference observed was related to the PEG length employed in each formulation. The material containing PEG4300 relaxed at longer times (τ = 514 s) than the networks containing PEG2100 (τ = 109 s for PU2100_HUB_1.5eq., 141 s for PU2100_HUB_1.25eq., and 306 s for PU2100_HUB_1.0eq.). Thus, it can be concluded that, among these three compositions, a higher dynamic bond ratio showed faster relaxation, and the PEG length is a key factor for the overall dynamicity of the materials. Considering these relaxation times, PU2100_HUB_1.5eq. has been chosen for the self-healing trials. This network showed the fastest stress-relaxation times in all the explored range of temperatures (80–140 °C).

Afterward, the self-healing behavior of the polyPU-HUB networks obtained by photopolymerization was assessed by optical microscopy. PU2100_HUB_1.5eq. was heated up to 60 and 50 °C under little pressure. These temperatures were both sufficient to surpass the melting temperature of PEG2100. As presented in Figure 2C, the healing process started in the first 15 min. However, it was not completed in such a short time. After 4 h, instead, total healing was almost achieved, and the sample continued the repairing phase up to 10 h, to finally exhibit a completely flat surface without visible scratches. Instead, at 50 °C the scratch was recovered after 8 h, and the complete initial shape was rearranged after 16 h.

2.3. DLP 3D Printing of PolyPU-HUB Networks

After confirming the preparation and repairability of the material, DLP photopolymerization was used to obtain 3D-printed figures of the polyPU-HUB networks. As illustrated in **Figure** 3A, this procedure initiates with a liquid photo-crosslinkable resin, which is irradiated using UV-light. This action induced the crosslinking of the desired shape that is adhered to the platform while this moved along the *Z*-axis from bottom to top, building the final object in a layer-by-layer process.

One of the key requirements for successful DLP printing is that the viscosity of the resin must be low (i.e., $\eta \approx 0.2$–10 Pa s).[42] For this reason, although polyPU-HUB ink showed the ability to form membranes by photopolymerization, it was not suitable for complex architecture printing due to its higher viscosity, and

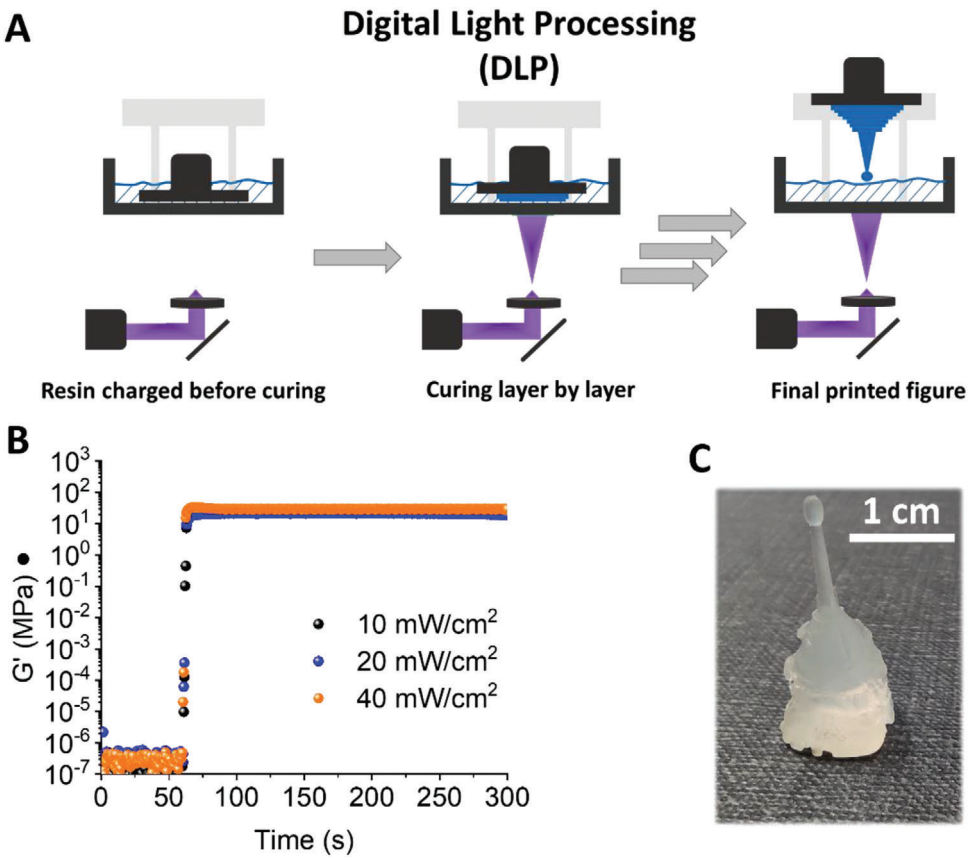

Figure 3. A) Scheme of the DLP technique showing the main workflow for the fabrication of 3D objects. B) Photorheometry measurements of PEG575 + PU2100_HUB_1.5eq. (80/20 wt/wt) formulation. C) Representative image of a 3D printed figure design, i.e., Mole Antonelliana building in Turin (Italy), scale bar 1 cm.

therefore low recoating efficiency. To enhance the resin printability, a low-viscosity reactive diluent (i.e., poly(ethylene glycol) diacrylate–PEGDA, M_n 575 g mol^{-1}) was added to facilitate the printing of PEGDA575/PU2100_HUB_1.5eq. (80/20 wt:wt), together with a photoinitiator (i.e., DMPA 1 wt.%). All the components of the resin were stirred in the darkness at room temperature, obtaining a transparent resin of the correct viscosity for its printing. Upon UV-light irradiation, the resin cures through well-established free-radical polymerization of radical-sensitive (meth)acrylate groups, provoking the solidification of the resin.

Before printing, photo-rheology experiments were performed using a UV-light accessory bearing an LED centered at 365 nm and under different light intensities (i.e., 10, 20, and 40 mW cm^{-2}), to optimize printing conditions and to see the effect of the irradiation intensity on the crosslinking kinetic (Figure 3B). At all irradiation intensities, the material showed extremely fast crosslinking kinetics, with storage modulus (G') over loss modulus (G'') crossover times lower than 1 s in all cases. Therefore, it seems that the irradiation intensity does not have much effect on the crosslinking rate. Besides, the plateau G' after irradiation was in all the cases between 20 and 30 MPa, suggesting equivalent network formation in all the cases. Therefore, among the tested intensities, 10 mW cm^{-2} was used to print this material, since it seemed to be sufficient to induce fast photocuring of the resin. Besides, layer exposure time and first layer exposure time were determined as previously reported using Jacob's working curve,[43] first layer irradiation time was found to be 5 s, while 0.9 s normal layer exposure time was chosen for layers of 50 µm. With these printing conditions, high-resolution 3D structures were printed in fast times (i.e., the Mole Antonelliana building shown in Figure 3C was printed in 97 min, this being 21 mm high). It must be added that the high Z-axis resolution obtained by VP (i.e., 50 µm) increases the reproducibility of electrolyte preparation while keeping a high productivity rate. After the printing process, the uncured resin was removed using isopropyl alcohol, and the final product was post-cured under UV (Asiga Flash UV curing chamber) for 5 min.

2.4. Electrochemical Characterization of PolyPU-HUB Networks as Polymer Electrolytes

For the complete electrochemical characterization of UV-cured membranes, prepolymer mixtures of each composition were deposited in molds and cured for 1 min under UV light. The crosslinked poly(urea-urethane) membranes were die-cut into 12 mm diameter small discs. Then, the swelling process was performed in a commercially available $LiPF_6$ 1 M solution in ethylene carbonate and diethyl carbonate (EC:DEC) 1:1 mixture; finally, a self-healable gel-polymer electrolyte with a

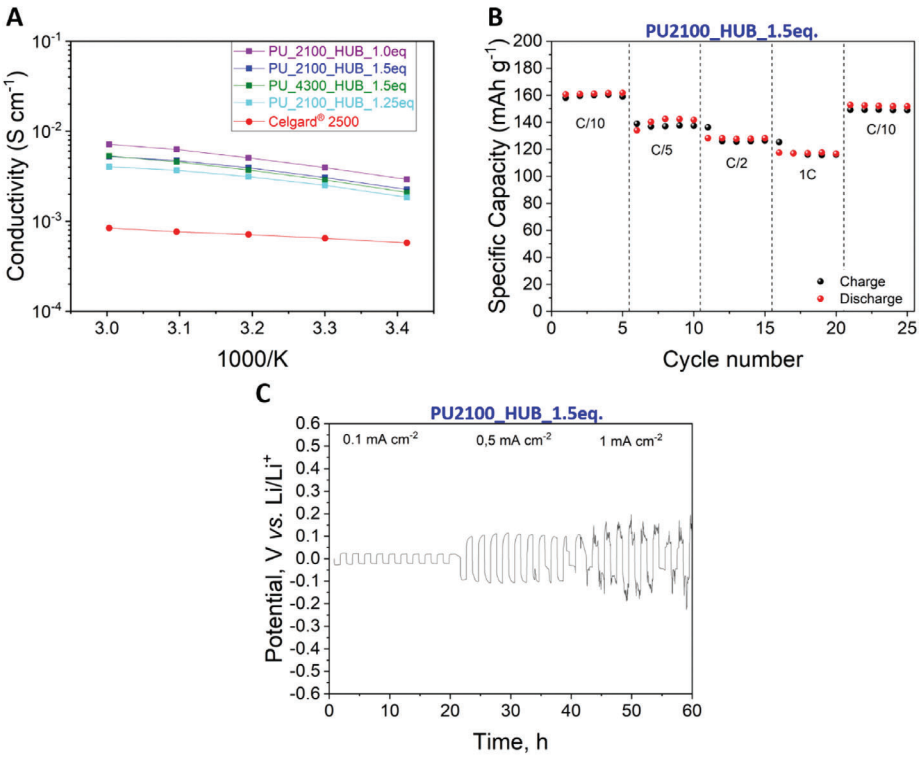

Figure 4. A) Ionic conductivity values at different temperatures for the polyPU-HUB networks and Celgard 2500 systems. B) Rate performance of a cell assembled with the PEG2100_HUB_1.5eq. composition. C) Potential versus test time of Li^+ stripping and plating for a symmetrical Li/Li cell at various current densities and at room temperature for the PU2100_HUB_1.5eq. composition.

diameter of 18 mm was obtained. These membranes were tested as polymer electrolytes in different cell configurations: i) symmetrical stainless steel|polymer electrolyte|stainless steel cells were used to measure the ionic conductivity; ii) Li-metal|polymer electrolyte|Li-metal cells were assembled to investigate the transference number and the Li^+ ion plating and stripping behavior; iii) Li-metal|polymer electrolyte|$LiFePO_4$ half-cells were prepared to assess the cycling performances (i.e., charge/discharge tests) in lab-scale prototypes.

Concerning one of the most decisive features of an electrolyte, the ionic conductivity values were measured between 20 and 60 °C for all the novel compositions and for the well-known, commercially available Celgard 2500 polyolefin-embedded porous separator. The synthesized polymer electrolytes showed, for each composition, a conductivity value almost one order of magnitude higher than that of the commercial separator, as shown in **Figure** 4A. The poly(urea-urethane) membranes showed close conductivity values among them, but the composition with the lowest amount of HUB dynamic bonds led to the highest values in the whole temperature range. Probably, this stoichiometrically adjusted material possesses well-distributed chains, which allows a homogeneous entrapment of the liquid electrolyte in the membrane matrix, facilitating Li^+ conduction. The compositions with increasing amounts of HUBs (from 1.25 eq. up to 1.5 eq.) showed lower but very similar values, regardless of the employed PEG length. In this case, hard segment sections are distributed more irregularly and the Li^+ conductive pathways across the membrane are not so well distributed and defined as in the PU2100_HUB_1.0eq. sample. Nevertheless, the second-best conductivity trend was achieved by PU2100_HUB_1.5eq. sample, as a result of a compromise between the dynamicity of the HUBs and the mechanical stiffness provided by their hard segments.

The electrochemical effect of the perfect distribution of the PU2100_HUB_1.0eq. chains versus the compromise in the PU2100_HUB_1.5eq. is also qualified by the higher Li^+ transference number (t_{Li^+}) of the former sample with respect to the latter (i.e., 0.49 vs 0.29, determined by Bruce–Vincent's method). The stoichiometrically adapted matrix of PU2100_HUB_1.0eq. allows a perfectly homogeneous flux of Li^+ ions across its thickness, providing the highest t_{Li^+} value; nevertheless, the most promising polymer electrolyte should be the one possessing the best trade-off between the ability to conduct ions and the mechanical properties to manage continuous charge flux and volume changes of the entire system. Indeed, the dynamicity witnessed by its fastest relaxation time indicates the PU2100_HUB_1.5eq. as the best-performing electrolyte during the plating and stripping test. In the symmetric cell, a continuous flux of Li^+ migrates from one lithium metal electrode to the other, and vice versa depending on the sign of the applied current. The recorded overpotential depends on the resistance at the interfaces between the electrolyte and the electrodes. Its value and shape can give a detailed insight into the polymer membrane's performance as an electrolyte. The PU2100_HUB_1.5eq. gel electrolyte showed the most desirable plating and stripping behavior among the four explored compositions; opposing the lowest resistance to the Li^+ transference, it results in the lowest

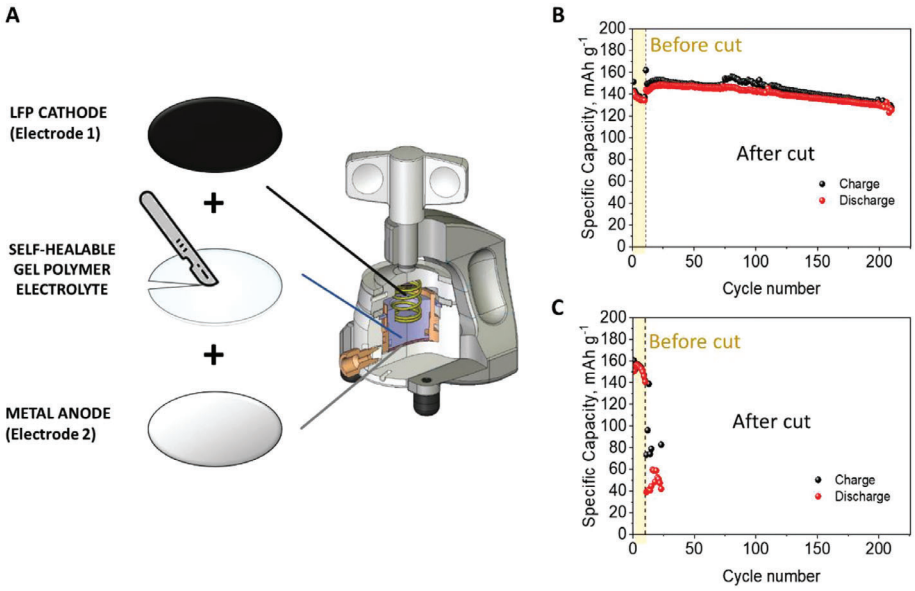

Figure 5. A) Cell disassembling and polymer electrolyte scratching step to carry out an in operando self-healing test (i.e., during the electrochemical test of the Li-metal cell). B) Charge/discharge test at C/5 of the cell assembled with the 3D-printed PU2100_HUB_1.5eq. polymer electrolyte, before and after the mechanical damage of the membrane. C) The same experiment was carried out with a commercial Celgard 2500 separator.

overpotential (Figure 4C) with respect to the other formulations (Figure S5, Supporting Information). Indeed, as the above-mentioned stress-relaxation time of the rheological results increases (from PU2100_HUB_1.5eq. to PU2100_HUB_1.25eq., PU2100_HUB_1.0eq., and PU4300_HUB_1.5eq.), so does the overpotential of the four systems. The highest dynamicity of PU2100_HUB_1.5 eq. guarantees also aligned plating and stripping profile shapes as the current density rises from 0.1 to 1 mA cm^{-2}; meanwhile, the balanced stiffness, also provided by the higher amount of HUBs, avoids the occurrence of relevant peaks in the overpotential profile, which would have otherwise indicated the growth of lithium dendrites. In general, these findings showcased a significantly smoother plating and stripping profile for the PU2100_HUB_1.5eq electrolyte, suggesting suppressed growth of lithium dendrites and great reversibility of Li^+ ions plating and stripping.

To study the cycling performance of the self-healable poly(urea-urethane) networks and to compare them with a commercial Celgard 2500 separator, lithium metal-based half-cells with $LiFePO_4$ (LFP) as a cathode were assembled and tested at room temperature. Figure 4B presents the cell performances at increasing specific currents (from C/10 to 1C) in the presence of the PU2100_HUB_1.5 eq network. The electrochemical performance exhibited by the latter is the most impressive. Figures S6 and S7 (Supporting Information) show the rate performances for the four poly(urea-urethane) compositions and the Celgard 2500 system, respectively. As predictable, among these five systems, Figures S6 and S7 (Supporting Information) show that PU_2100_HUB_1.0eq., PU2100_HUB_1.5eq, and the commercial separator provided the highest (and very close among them) specific capacities. The most prompt electrochemical response to the current rate increase was achieved by the PU2100_HUB_1.5eq. sample, in light of its fastest mechanical response to the continuous stress–strain previously discussed. Indeed, the fastest chain rearrangement of PU2100_HUB_1.5eq. electrolyte allowed, at the 21th cycle, the immediate retainment of 95% of the first cycle discharge capacity, when the C-rate is brought back to C/10; its thermal stability under air atmosphere is also shown in Figure S8 (Supporting Information), highlighting a truly high resistance of the polymeric backbone in the common temperature operative range of LMBs. In parallel, the Celgard 2500 membrane retained 85% of the initial value (data not reported), while PU_2100_HUB_1.0eq. kept the 75%.

2.5. Self-Healing During Electrochemical Tests

As explained in the previous sections, controlled thin membranes of the hindered poly(urea-urethane) networks containing PEG2100 are affordable due to the low printing times necessary to completely cure 100 µm-thick discs. These materials have been selected considering the results from our previous electrochemical characterization and stress-relaxation measurements. The PU2100_HUB_1.5eq.-based polymer electrolyte was then electrochemically tested for 10 charge/discharge cycles at C/5 rate before being disassembled and mechanically scratched with a surgeon knife in the glovebox (**Figure 5A**). Then, the electrochemical cell was reassembled, and without any thermomechanical treatment, the charge/discharge test was re-started at the same C/5 rate at room temperature. The first values of the specific capacity recorded just after membrane damage were surprisingly superior to those related to the formerly undamaged membrane; we carried out this experiment in five replicas and this behavior was fully reproducible. Probably, due to the highly dissociative behavior of the HUBs, the material is not totally well healed at this stage and has more free channels available for Li^+ movement and possible lithium plating near the damage, causing this superior capacity. Nevertheless, the healing process

naturally continued during the subsequent charge and discharge cycles, and the polymer electrolyte reached complete recovery up to the nullification of the excess capacity of the first post-cut cycles (Figure 5B). Conversely, the commercially available electrolyte Celgard 2500 (Figure 5C), which underwent the same protocol, failed a few cycles after the membrane cut due to the growth of dendrites that led to cell short-circuit. The novel 3D-printed electrolyte showed great specific capacity values, and marvelous self-healing properties, and retained 91% of the discharge capacity recorded at the first cycle after as many as 200 cycles; a rate-capability test is also shown in Figure S9 (Supporting Information). The presence of a scratch on the solid polymeric matrix represents for Li-ions a kinetically enhanced pathway, with lower resistance on the overall electrolyte thickness, and, thus, a hotspot for the lithium plating and the dendrite growth. However, such a high capacity retention proved the achievement of the damage healing prior to the growth of the dendrite to the point of no return. This result stands out in the field of self-healing polymer electrolytes (e.g., dynamic boronic ester bonds-based,[44] siloxane networks,[45] methacrylates,[42] ionic liquids-laden polymers,[46] etc.), both in terms of durability and for the ability to make cell work even after a membrane cut.

The previous plating and stripping test demonstrated that the best composition of PU2100_HUB_1.5eq. can deliver the most performant potential profile when conducting Li^+ ions forward and backward at increasing current density under ideal conditions. However, the primary scope of this work is to propose a quasi-solid polymer electrolyte capable of self-healing its damages before the formation of fully grown metal dendrites. Therefore, the 3D-printed PU2100_HUB_1.5eq. electrolyte underwent an additional plating and stripping experiment. In this case, the symmetrical Li-metal|polymer electrolyte|Li-metal cell was assembled with a slightly damaged 3D-printed PU2100_HUB_1.5eq. and tested at the constant current density of 0.5 mA cm^{-2} for 300 h at room temperature. In **Figure 6**, the novel 3D-printed membrane effectively withstood the challenging current and test duration without any short circuits. Notably, voltage spikes were observed during the initial cycles, representative of the nucleation of lithium dendrites near the damaged area, which confirms the theory of the higher capacities shown in Figure 5B during the first post-damage cycles. Subtle, but relevant, it is the presence of the peaks only in the upper potential window, where the nucleation on the Li-metal occurs, only at the damaged interface. Nevertheless, these peaks diminished in the subsequent cycles, disappearing into a symmetric and regular potential curve, suggesting that the scratch healed before causing irreversible damage. Subsequently, a constant overpotential, higher than that of the undamaged PU2100_HUB_1.5eq. shown in Figure 4B (i.e., 0.5 vs 0.1 V vs Li^+/Li), was reached, resulting from the less homogenous interface formed during the initial healing cycling. Nonetheless, as illustrated in the inset of Figure 6, the potential profile of the post-healing cycles recovered and was preserved for the remaining test duration.[47]

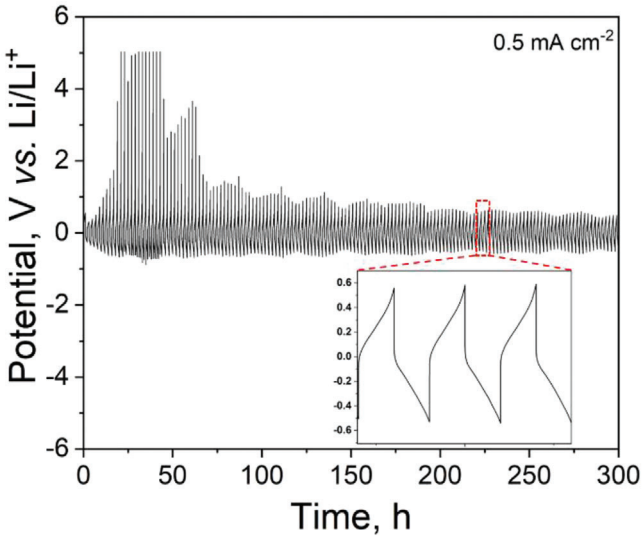

Figure 6. Plating and stripping tests were carried out at constant current density on a Li/Li symmetrical cell assembled with a slightly damaged PU2100_HUB_1.5eq. electrolyte. In the inset, the potential profiles of 3 cycles after the interface stabilization are zoomed.

3. Conclusion

In this work, the development of covalent adaptable networks containing hindered urea dynamic bonds as self-healable and 3D-printable polymer electrolytes for LMBs is reported. The CAN chemistry was tailored to be compatible with UV-light photopolymerization through the design of a new family of hindered-urea dimethacrylate oligomers.

The dynamicity of the CAN formulations was investigated by rheological studies. Fast stress-relaxation times were obtained with raw formulations, directly related to the dynamic bond concentration. According to these results, self-healing properties were studied by optical microscopy for the most dynamic formulation (i.e., PU2100_HUB_1.5eq.). Then, new membranes and 3D-printing objects were obtained by fast UV-light curing. The electrochemical performance of polymer electrolytes formulated for LMBs was assessed and compared with those recorded with a commercially available separator (i.e., Celgard 2500), showing in all cases superior ionic conductivities and cycling performances.

The most promising formulation was selected to fabricate thickness-controlled separators polymer electrolyte membranes by VAT photopolymerization. The potential advantage of the self-healing ability of the hindered-urea CANs was demonstrated by opening a lab-scale LMB cell and cutting the polymer electrolyte. Notably, the self-healing CAN keep high capacity values after recovery from the cut, showing a great performance even after 200 cycles. In contrast, in the case of the commercially available separator, the capacity values rapidly dropped after the scratching.

Overall, these findings contribute to the implementation of new self-healing polymer chemistries such as hindered-urea CANs as safe solid (or quasi-solid) electrolytes for batteries. Furthermore, this work paves the way for lab-scale research into a manufacturing method that allows to scan and optimize the polymer electrolyte thickness, finding the threshold between ionic conductivity and mechanical support; also, it makes another step further, showing for the first time that self-healable electrolytes can be manufactured by VAT photopolymerization, thus being compatible with 3D-printing processes in the new-generation

battery gigafactories, as well as lithium-mediated ammonia electrosynthesis.

4. Experimental Section

Chemicals and Materials: *N,N'*-di-tert-butylethylenediamine, dibutyltin dilaurate (DBTDL, 95%), hexamethylene diisocyanate (HDI, ≥98.0%), anhydrous tetrahydrofuran (THF, ≥99.9%), 2,2-dimethoxy-2-phenylacetophenone (DMPA, 99%), poly(ethylene glycol) diacrylate (PEGDA, M_n 575 g mol^{-1}), and 2-hydroxyethyl methacrylate (HEMA, ≥97.0%) were purchased from Merck and used as received. PEG2100 and PEG4300 were purchased from Merck and dried in the oven (70 °C) overnight before use. $LiPF_6$ 1.0 M solution in EC:DEC (1:1 v:v) was purchased from Solvionic and used in the glovebox. Poly(vinylidene difluoride) (PVDF) as polymer binder (HSV 900:ADX 160 90:10 wt.%) was acquired from Arkema, and used at 10 wt.% in *N*-methyl-2-pyrrolidinone (NMP). This latter, along with lithium disks (Chemetall Foote Corporation, Ø 16 mm), poly(propylene) polymeric membrane Celgard 2500 (25 µm-thickness, Ø 19 mm), $LiFePO_4$ (Aleees), and carbon black powder (C65, C-NERGY Super C65, Timcal), was used as received.

Synthesis of PU2100_HUB and PU4300_HUB Membranes: To synthesize self-healable crosslinked poly(urea-urethane) networks, let's take PU2100_HUB1.5eq. as a representative example. *N,N´*-di-*tert*-butylethylenediamine (0.56 mmol, 97 mg, 121 µL) was added dropwise to HDI (0.94 mmol, 158 mg) to form free isocyanate group end-capped hindered urea dimmers and redissolved in a little amount of anhydrous THF (1 mL). The solution was kept stirring at room temperature for 15 min. Previously dried PEG2100 (0.19 mmol, 400 mg) was then added to the solution at 65 °C. Once PEG was properly mixed, DBTDL (2 mol% with respect to the –NCO content, 0.019 mmol, 11 µL) was added and, after 10 min stirring, HEMA (0.37 mmol, 49 mg, 45.5 µL) was introduced to the end cap poly(urea-urethane) chains. The photoinitiator DMPA (5 wt.%) was added in this step. The mixture was placed in a circular Teflon mold. The curing step (1 min) was performed by UV-light after THF evaporation in the oven (15 min). The VAT photocuring was performed as explained in Figure 3A.

All the compositions synthesized for this work were summarized in Tables S1–S5 (Supporting Information). To obtain thin membranes for battery applications by VAT photopolymerization, these resins were used without further modifications. Instead, to create more complex 3D structures, each formulation has to be tuned as explained in the next section.

Synthesis of PU2100_HUB Containing 3D Printable Resin Mixture: Previously synthesized PU2100_HUB1.5eq. was mixed with PEGDA (20/80 wt.%) to create a non-crystallizing resin. This mixture was used for 3D-printing more complex geometries, such as the one shown in Figure 3C using a Asiga Max-UV commercial DLP printer.

Characterization of Poly(Urea-Urethane) Membranes: ^{1}H-NMR spectroscopy data were recorded on a 300 MHz Bruker Advance DPX spectrometer at 20 °C. The samples were dissolved in deuterated chloroform and chemical shifts were reported in ppm referenced to solvents peaks. FTIR spectra were recorded on a Nicolet iS20 Spectrometer using attenuated total reflection at a resolution of 2 cm^{-1} and a total of 32 interferograms. Photo-DSC analyses were performed in a DSC25 from TA instruments coupled to a custom photocalorimetric accessory, using a Kessil UV-LED light-emitting lamp centered at 370 nm. Isothermal experiments were conducted using ≈1.5 mg of sample. Calculation of functional group conversion was performed using the area under the integral of the exothermic peak, as previously reported.[48]

Cathode Preparation: To prepare the $LiFePO_4$ electrode as a cathode for cell testing, a slurry consisting of $LiFePO_4$, C65, and PVDF was prepared at a 70:20:10 weight ratio, using NMP as a solvent. Then, the slurry (homogenized in a mixer mill, Retsch MM40) was coated onto an aluminum foil with a doctor blade film applicator and dried overnight at room temperature. The resulting electrode was then cut into discs of 15 mm-diameter and subjected to vacuum drying at 120 °C for 4 h (Büchi Glass Oven B-585) and stored in an argon-filled glovebox (MBraun Labstar, H_2O and O_2 content < 1 ppm) for cell assembly.

Membrane Activation: The different membranes prepared in this work were cut into 12 mm discs, dried under vacuum at 50 °C for 12 h, and then transferred into a glovebox to be activated by swelling in a $LiPF_6$ 1.0 M solution in EC:DEC (1:1 v:v) for 40 min. For the membrane containing PEG4300, the swelling time was 1 h.

Stress Relaxation Measurements: Stress relaxation experiments to obtain the relaxation modulus E(t) were carried out by an ARES rheometer (Rheometrics) under the conditions indicated in the manuscript, using a film tension fixture and 5% strain. Employed samples had a width between 1.20 and 2.05 mm, and a thickness between 0.15 and 0.35 mm.

Photorheometry Measurements: The rheometer AR-G2 (TA Instruments) was used, equipped with a 365 nm ultraviolet light emission accessory of variable intensity. A 20 mm-diameter upper parallel plate geometry was used, with a transparent acrylic bottom plate to let the irradiation pass through. A gap value of 300 µm was used. The measurements were carried out at 60 °C (to keep the material melted) and in the linear viscoelasticity zone (i.e., at deformations where the structure of the material was not altered) so that measurements were comparable with each other. To monitor the effect of the light irradiation intensity on the photocuring of the resin, measurements were made at 10, 20, and 40 mW cm^{-2}. Irradiation was initiated after 60 s.

Electrochemical Characterization: The electrochemical testing was carried out to compare the newly designed polyPU-HUB membrane with a commercial separator (i.e., Celgard 2500) impregnated with 300 µL of the above-mentioned liquid electrolyte.

The ionic conductivity was determined by electrochemical impedance spectroscopy (EIS) in the frequency range between 100 kHz and 1 Hz at open circuit potential, using a VSP-3e potentiostat (BioLogic). The activated membrane was sandwiched between two stainless steel blocking electrodes (ECC-Std test cells by EL-CELL GmbH). The assembled cells were kept in a climatic chamber (model MK53 E2.1 by BINDER GmbH) and tested between 20 and 60 °C. The resistance of the electrolyte was given by the high-frequency intercept of the Nyquist's plot. The ionic conductivity was calculated at each temperature using Equation (1):

$$\sigma = (l/A) \times \left(1/R_b\right) \quad (1)$$

where l is the membrane thickness, A is the membrane surface area, and R_b is the resistance value at the high-frequency intercept.

The transference number was measured by Bruce, Vincent, and Evans method.[49] A CR2032 coin cell was assembled with two lithium foil sandwiching the tested electrolyte. An EIS experiment between 100 kHz and 0.1 Hz was carried out before and after applying a constant polarization potential of 10 mV, measuring the initial (I_o) and the steady-state (I_s) current values, as well as the initial (R_0) and the steady-state (R_s) interfacial impedance values. The lithium transference number was calculated according to this equation:

$$t_{Li^+} = \frac{I_s(\Delta V - I_0 R_0)}{I_0(\Delta V - I_s R_s)} \quad (2)$$

The electrochemical stability window (ESW, data not shown) was assessed by linear sweep voltammetry (LSV), carried out onto a stainless steel|polyPU-HUB membrane|Li-metal cell by a potentiostat (CH Instruments, Inc.), at a scan rate of 0.5 mV s^{-1} from 0.5 to 6 V versus Li^+/Li at room temperature.

The effect of the membrane on Li^+ plating and stripping was studied using a Li-metal/Li-metal symmetrical cell configuration, with the polyPU-HUB membrane sandwiched in between and using the VSP-3e potentiostat. The current density and the related discharge capacity were 0.1 mA cm^{-2} and 0.1 mAh cm^{-2}, 0.5 mA cm^{-2} and 0.5 mAh cm^{-2}, 1 mA cm^{-2} and 1 mAh cm^{-2}, respectively. A EIS measurement was performed, between 100 kHz and 1 Hz at open circuit potential, on fresh cells and after 10 cycles at each current density.

For lab-scale prototype testing, cells with an architecture based on $LiFePO_4$|polyPU-HUB membrane|Li-metal were assembled. Galvanostatic cycling was performed to assess lifetime and rate performances on an Arbin BT-2000 battery tester. The tests were carried out at room temperature and the charge/discharge rates were based on the $LiFePO_4$ theoretical specific capacity of 170 mAh g^{-1}. The same configuration was used to assess the self-healing capability of the PU2100_HUB_1.5eq. and the impregnated Celgard 2500 galvanostatic cycling the cells for 10 cycles at C/5, disassembled, scratched with a knife, and reassembled to keep cycling at the same C-rate for 200 cycles. With the same purpose, a symmetrical Li/Li cell assembled with a slightly damaged PU2100_HUB_1.5eq. electrolyte underwent 300 h of plating and stripping at 0.5 mA cm^{-2}.

Each electrochemical measurement described in this section was conducted in at least three replicates.

Supporting Information

Supporting Information is available from the Wiley Online Library or from the author.

Acknowledgements

F.E. and S.T. contributed equally to this work. This project has received funding from the European Research Council (ERC) under the European Union's Horizon 2020 research and innovation program (grant agreement No. 948769, project title: SuN_2rise).

Open access publishing facilitated by Politecnico di Torino, as part of the Wiley - CRUI-CARE agreement.

Conflict of Interest

The authors declare no conflict of interest.

Data Availability Statement

The data that support the findings of this study are available from the corresponding author upon reasonable request.

Keywords

3D printing, hindered urea dynamic bonds, lithium battery, polymer electrolyte, self-healing

Received: October 29, 2024
Revised: November 11, 2024
Published online: December 1, 2024

[1] D. Chen, D. Wang, Y. Yang, Q. Huang, S. Zhu, Z. Zheng, *Adv. Energy Mater.* **2017**, *7*, 27.
[2] C. Gu, M. Wang, K. Zhang, J. Li, Y. L. Lu, Y. Cui, Y. Zhang, C. S. Liu, *Adv. Mater.* **2023**, *35*, 2208392.
[3] Y. Fan, T. Tao, Y. Gao, C. Deng, B. Yu, Y. Chen, S. Lu, S. Huang, *Adv. Mater.* **2020**, *32*, 2004798.
[4] A. S. Aricò, P. Bruce, B. Scrosati, J. M. Tarascon, W. Van Schalkwijk, *Nat. Mater.* **2005**, *45*, 366.
[5] J. Zhang, H. Zhang, S. Weng, R. Li, D. Lu, T. Deng, S. Zhang, L. Lv, J. Qi, X. Xiao, L. Fan, S. Geng, F. Wang, L. Chen, M. Noked, Z. Wang, Z. Fan, *Nat. Commun.* **2023**, *14*, 2211.
[6] H. Zhang, H. Zhao, M. A. Khan, W. Zou, J. Xu, L. Zhang, J. Zhang, *J. Mater. Chem. A* **2018**, *6*, 20564.
[7] S. Wang, T. Cheng, Y. Z. Zhang, X. Wu, S. Xiao, W. Y. Lai, *Appl. Phys. Rev.* **2022**, *9*, 041310.
[8] G. Zubi, R. Dufo-López, M. Carvalho, G. Pasaoglu, *Renew. Sustain. Energy Rev.* **2018**, *89*, 292.
[9] D. Lin, Y. Liu, Y. Cui, *Nat. Nanotechnol.* **2017**, *12*, 194.
[10] Y. Wu, X. Li, G. Yan, Z. Wang, H. Guo, Y. Ke, L. Wu, H. Fu, J. Wang, *J. Energy Chem.* **2020**, *53*, 116.
[11] Z. Wang, J. Liu, M. Wang, X. Shen, T. Qian, C. Yan, *Nanoscale Adv.* **2020**, *2*, 1828.
[12] A. Mangini, L. Fagiolari, A. Sacchetti, A. Garbujo, P. Biasi, F. Bella, *Adv. Energy Mater.* **2024**, *14*, 2400076.
[13] M. Gandolfo, D. Versaci, C. Francia, S. Bodoardo, J. Amici, *Electrochim. Acta* **2023**, *463*, 142857.
[14] P. Ding, Z. Lin, X. Guo, L. Wu, Y. Wang, H. Guo, L. Li, H. Yu, *Mater. Today* **2021**, *51*, 449.
[15] E. R. Ezeigwe, L. Dong, R. Manjunatha, M. Tan, W. Yan, J. Zhang, *Nano Energy* **2021**, *84*, 105907.
[16] B. Zhou, D. He, J. Hu, Y. Ye, H. Peng, X. Zhou, X. Xie, Z. Xue, *J Mater. Chem. A* **2018**, *6*, 11725.
[17] L. Mezzomo, C. Ferrara, G. Brugnetti, D. Callegari, E. Quartarone, P. Mustarelli, R. Ruffo, *Adv. Energy Mater.* **2020**, *10*, 2002815.
[18] Y. Cheng, X. Xiao, K. Pan, H. Pang, *Chem. Eng. J.* **2020**, *380*, 122565.
[19] T. Munaoka, X. Yan, J. Lopez, J. W. F. To, J. Park, J. B. H. Tok, Y. Cui, Z. Bao, *Adv. Energy Mater.* **2018**, *8*, 1703138.
[20] S. Siccardi, J. Amici, S. Colombi, J. T. Carvalho, D. Versaci, E. Quartarone, L. Pereira, F. Bella, C. Francia, S. Bodoardo, *Electrochim. Acta* **2022**, *433*, 141265.
[21] F. Elizalde, J. Amici, S. Trano, G. Vozzolo, R. Aguirresarobe, D. Versaci, S. Bodoardo, D. Mecerreyes, H. Sardon, F. Bella, *J. Mater. Chem. A* **2022**, *10*, 12588.

[22] B. Zhou, T. Deng, C. Yang, M. Wang, H. Yan, Z. Yang, Z. Wang, Z. Xue, *Adv. Funct. Mater.* **2023**, *33*, 2212005.
[23] Z. Sun, J. Wu, H. Yuan, J. Lan, Y. Yu, Y. Zhu, X. Yang, *Mater. Today Energy* **2022**, *24*, 100939.
[24] H. Ying, Y. Zhang, J. Cheng, *Nat. Commun.* **2014**, *5*, 3218.
[25] J. Herzberger, J. M. Sirrine, C. B. Williams, T. E. Long, *Prog. Polym. Sci.* **2019**, *97*, 101144.
[26] H. Yuk, B. Lu, S. Lin, K. Qu, J. Xu, J. Luo, X. Zhao, *Nat. Commun.* **2020**, *11*, 4.
[27] M. A. Saccone, Vat photopolymerization additive manufacturing of functional materials: from batteries to metals and alloys, Dissertation (Ph.D.), at the California Institute of Technology, **2022**, https://doi.org/10.7907/v3cn-8h28.
[28] M. Cong, Y. Du, Y. Liu, J. Xu, K. Zhao, F. Lian, T. Lin, H. Shao, *Ceram. Int.* **2024**, *50*, 14749.
[29] J. Fu, D. Wang, Y. Li, X. Liu, R. Zhang, Z. Liu, P. Liu, L. Zhang, X. Li, G. Wen, *Nano Res.* **2024**, *17*, 2693.
[30] A. G. Sabato, M. Nuñez Eroles, S. Anelli, C. D. Sierra, J. C. Gonzalez-Rosillo, M. Torrell, A. Pesce, G. Accardo, M. Casas-Cabanas, P. López-Aranguren, A. Morata, A. Tarancón, *J. Mater. Chem. A* **2023**, *11*, 13677.
[31] X. Hu, Y. Chen, W. Xu, Y. Zhu, D. Kim, Y. Fan, B. Yu, Y. Chen, *Small* **2023**, *19*, 2301604.
[32] S. Huo, L. Sheng, B. Su, W. Xue, L. Wang, H. Xu, X. He, *Adv. Mater.* **2024**, *36*, 2310396.
[33] Y. Pang, Y. Cao, Y. Chu, M. Liu, K. Snyder, D. Mackenzie, *Adv. Funct. Mater.* **2020**, *30*, 1906244.
[34] A. Maurel, A. N. A. C. Martinez, S. Grugeon, S. Panier, S. T. Sreenivasan, E. Macdonald, *IEEE Access* **2021**, *9*, 140654.
[35] P. Chang, H. Mei, S. Zhou, K. G. Dassios, L. Chenga, *J. Mater. Chem. A* **2019**, *7*, 4230.
[36] D. W. Yee, J. R. Greer, *Polym. Int.* **2021**, *70*, 964.
[37] A. Ambrosi, M. Pumera, *Chem. Soc. Rev.* **2016**, *45*, 2740.
[38] Z. Lyu, G. J. H. Lim, J. J. Koh, Y. Li, Y. Ma, J. Ding, J. Wang, Z. Hu, J. Wang, W. Chen, Y. Chen, *Joule* **2021**, *5*, 89.
[39] K. Lee, Y. Shang, V. A. Bobrin, R. Kuchel, D. Kundu, N. Corrigan, C. Boyer, *Adv. Mater.* **2022**, *34*, 2204816.
[40] F. Zhang, L. Zhu, Z. Li, S. Wang, J. Shi, W. Tang, N. Li, J. Yang, *Addit. Manuf.* **2021**, *48*, 102423.
[41] Q. Zhang, S. Wang, B. Rao, X. Chen, L. Ma, C. Cui, Q. Zhong, Z. Li, Y. Cheng, Y. Zhang, *React. Funct. Polym.* **2021**, *159*, 104807.
[42] J. W. Choi, G. J. Kim, S. Hong, J. H. An, B. J. Kim, C. Q. Ha, *Sci. Rep.* **2022**, *12*, 13553.
[43] M. Štaffová, F. Ondreáš, J. Svatík, M. Zbončák, J. Jančář, P. Lepcio, *Polym. Test.* **2022**, *108*, 107499.
[44] S. Zhou, X. Wang, Z. Xu, T. Guan, D. Mo, K. Deng, *J. Energy Storage* **2024**, *75*, 109712.
[45] Y. Chen, C. Ling, K. Long, X. Liu, P. Xiao, Y. Z. Yu, W. Wei, X. Ji, W. Tang, G. C. Kuang, L. Chen, *Chem. Eng. J.* **2024**, *488*, 150888.
[46] J. Wu, Y. Sun, T. Wu, Y. Zhu, Y. Zhu, C. Lai, *Electrochim. Acta* **2024**, *492*, 144361.
[47] C. Fu, G. Homann, R. Grissa, D. Rentsch, W. Zhao, T. Gouveia, A. Falgayrat, R. Lin, S. Fantini, C. Battaglia, *Adv. Energy Mater.* **2022**, *12*, 2200412.
[48] O. Llorente, M. J. Fernández-Berridi, A. González, L. Irusta, *Prog. Org. Coat.* **2016**, *99*, 437.
[49] J. Evans, C. A. Vincent, P. G. Bruce, *Polymer* **1987**, *28*, 2324.